BIOCHEMISTRY
including biophysical chemistry & molecular biology

Article

pubs.acs.org/biochemistry

O_2-Evolving Chlorite Dismutase as a Tool for Studying O_2-Utilizing Enzymes

Laura M. K. Dassama,[†] Timothy H. Yosca,[‡] Denise A. Conner,[‡] Michael H. Lee,[†] Béatrice Blanc,[§] Bennett R. Streit,[§] Michael T. Green,[‡] Jennifer L. DuBois,*[,§] Carsten Krebs,*[,†,‡] and J. Martin Bollinger, Jr.*[,†,‡]

[†]Department of Biochemistry and Molecular Biology and [‡]Department of Chemistry, The Pennsylvania State University, University Park, Pennsylvania 16802, United States

[§]Department of Chemistry and Biochemistry, University of Notre Dame, Notre Dame, Indiana 46556, United States

Supporting Information

ABSTRACT: The direct interrogation of fleeting intermediates by rapid-mixing kinetic methods has significantly advanced our understanding of enzymes that utilize dioxygen. The gas's modest aqueous solubility (<2 mM at 1 atm) presents a technical challenge to this approach, because it limits the rate of formation and extent of accumulation of intermediates. This challenge can be overcome by use of the heme enzyme chlorite dismutase (Cld) for the rapid, *in situ* generation of O_2 at concentrations far exceeding 2 mM. This method was used to define the O_2 concentration dependence of the reaction of the class Ic ribonucleotide reductase (RNR) from *Chlamydia trachomatis*, in which the enzyme's Mn^{IV}/Fe^{III} cofactor forms from a Mn^{II}/Fe^{II} complex and O_2 via a Mn^{IV}/Fe^{IV} intermediate, at effective O_2 concentrations as high as ~10 mM. With a more soluble receptor, myoglobin, an O_2 adduct accumulated to a concentration of >6 mM in <15 ms. Finally, the C−H-bond-cleaving Fe^{IV}−oxo complex, **J**, in taurine:α-ketoglutarate dioxygenase and superoxo−$Fe_2^{III/III}$ complex, **G**, in *myo*-inositol oxygenase, and the tyrosyl-radical-generating $Fe_2^{III/IV}$ intermediate, **X**, in *Escherichia coli* RNR, were all accumulated to yields more than twice those previously attained. This means of *in situ* O_2 evolution permits a >5 mM "pulse" of O_2 to be generated in <1 ms at the easily accessible Cld concentration of 50 μM. It should therefore significantly extend the range of kinetic and spectroscopic experiments that can routinely be undertaken in the study of these enzymes and could also facilitate resolution of mechanistic pathways in cases of either sluggish or thermodynamically unfavorable O_2 addition steps.

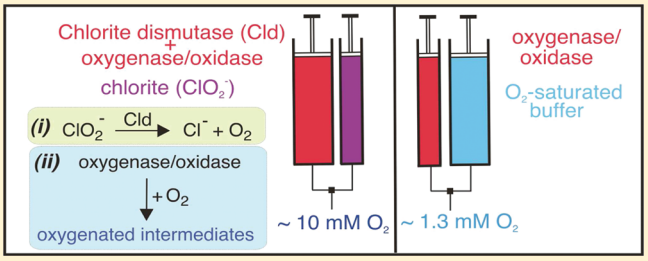

Aerobic organisms are replete with proteins and enzymes that react with O_2 for such purposes as cellular and organismal respiration;[1] oxidation reactions of primary and secondary metabolism;[2−4] catabolism of drug and xenobiotic compounds;[2] biosynthesis of enzyme cofactors,[5−7] neurotransmitters,[8] and natural products;[4,9] regulation of transcription;[10−13] and uptake and storage of inorganic nutrients.[14] Many of these enzymes employ reduced cofactors, consisting of one or more reduced transition metal (typically Fe^{II} [2,15−18] or Cu^{I} [19−21]) or a reduced flavin,[22] that combine with O_2 to form potently oxidizing intermediates that directly or indirectly transform their substrates. Rapid-mixing transient kinetic studies have contributed greatly to our understanding of the mechanisms of these enzymes by permitting the direct detection, kinetic tracking, and spectroscopic characterization of fleeting intermediates in their catalytic cycles.[15−18] The fleeting nature of the intermediates formed (typical half-lives of <1−10 s) has, with a few spectacular exceptions,[23−25] precluded their three-dimensional structural characterization by X-ray crystallography. The alternative approach has been (i) to trap the intermediates at their maximal extents of accumulation by the freeze-quench method and (ii) to subject them to a suite of spectroscopic methods. In combination with density functional theory (DFT) calculations,[26] these methods can afford local, high-resolution structural information about transient species, thereby providing "snapshots" along the reaction coordinate.[27−29]

In the study of these enzymes, the physical properties of O_2 impose certain challenges to the elucidation of reaction kinetics and the direct characterization of intermediates. Its gaseous nature makes systematic variation of its concentration more challenging and introduces greater uncertainty into concentration values than for nonvolatile substrates. More importantly, the modest solubility of the gas imposes a very constraining upper limit of ~2 mM on the O_2 concentration[30] that can be achieved without specialized apparatus. O_2 has often been found to combine with the reduced enzyme cofactors with second-order rate constants of 10^4−10^7 M^{-1} s^{-1}, which, at the routinely accessible O_2 concentration of 1 mM, are sufficient to

Received: December 21, 2011
Revised: January 18, 2012
Published: January 20, 2012

dx.doi.org/10.1021/bi201906x | *Biochemistry* 2012, 51, 1607−1616

give effective first-order rate constants of 10^1–10^4 s^{-1}.[31−34] In many cases, these formation rate constants have proven to be comparable to or greater than the first-order rate constants for decay of the key intermediates. In these cases, accumulation of the intermediate states for detailed characterization has been possible.[34−40] In other cases, isotopic or chemical modification of the substrate or mutagenesis of the protein has been used to slow decay of intermediates to permit their accumulation and characterization.[41−43] In still other cases, however, the obstacle presented by the modest solubility of O_2 has not been overcome, and many intriguing O_2-dependent enzyme reactions have thus far proven to be resistant to this powerful approach to mechanistic dissection.[44]

Several spectroscopic methods that can reveal important structural details for intermediates demand very concentrated samples that are highly enriched in the desired state. For example, application of extended X-ray absorption fine structure (EXAFS) spectroscopy, which in ideal cases can provide very precise metal−ligand and metal−metal distances for reactive intermediates, to dilute or heterogeneous freeze-quenched samples is notoriously problematic and in several notable cases has provided distances[45,46] that cannot be reconciled with those in DFT-derived structures[27,28,47] and inorganic model complexes.[48,49] Other methods, such as the developing technique of nuclear resonance vibrational spectroscopy (NRVS), which can reveal structural details of iron complexes, require that targets be present at concentrations exceeding the solubility of O_2.[50] Long-lived complexes may be generated at such high concentrations by direct treatment of precursors with gaseous O_2,[38,39] but the sluggishness of transport across the gas−liquid interface makes such an approach impractical for complexes with half-lives of less than ∼1 min. A rapid-mixing method permitting reaction with O_2 at greater concentrations without the need for specialized equipment could, therefore, open doors to new experiments in this area of biochemistry.

The heme enzyme chlorite dismutase (Cld) rapidly converts chlorite (ClO_2^-) to chloride (Cl^-) and O_2, suggesting a simple approach to overcoming both the technical difficulties in the systematic variation of O_2 concentration and its modest solubility.[51] A number of proteobacteria have been shown to catalyze this reaction in conjunction with perchlorate (ClO_4^-) respiration. ClO_4^- is sequentially reduced to ClO_3^- and ClO_2^- by a membrane-bound molybdopterin-dependent perchlorate reductase, which couples the reductions to the generation of a proton gradient.[52] The resulting ClO_2^- would accumulate and kill the organism in the absence of the detoxification reaction catalyzed by Cld. Accordingly, the reaction must be fast to serve its biological function: the homopentameric Cld from *Dechloromonas aromatica* (*Da*) is one of the fastest and most efficient Clds yet studied, with a k_{cat} value of (2.0 ± 0.6) × 10^5 s^{-1} (per heme) at 4 °C and pH 5.2.[51,53,54] This rate constant suggests that Cld could support the generation of tens-of-millimolar O_2 on the millisecond time scale. Importantly, the enzyme is not significantly inhibited by millimolar concentrations of either of its two products, Cl^- and O_2.[51] It is, moreover, capable of approximately 1.7 × 10^4 turnovers per heme before undergoing irreversible inactivation because of oxidative damage to the heme. We therefore reasoned that catalytic concentrations of Cld could be used to initiate the reaction of an O_2-utilizing (metallo)enzyme by rapid mixing with the highly soluble, nonvolatile ClO_2^- rather than with the sparingly soluble, gaseous O_2. Here, we demonstrate that this approach can indeed simplify the experimental variation of O_2 concentration, expand the range of O_2 concentrations that can be interrogated with commonly available equipment, and permit preparation of O_2-dependent intermediate states at concentrations and purities not accessible by conventional rapid mixing with O_2-containing aqueous solutions.

EXPERIMENTAL PROCEDURES

Materials. Sodium chlorite ($NaClO_2$), α-ketoglutaric acid, sodium ascorbate, and horse heart myoglobin (Mb) were purchased from Sigma-Aldrich. 1,1,2,2-[$^2H_4$]-2-Aminoethane-1-sulfonic acid (d_4-taurine) and 1,2,3,4,5,6-[$^2H_6$]-cyclohexan-(1,2,3,5/4,6)-*hexa*-ol (d_6-*myo*-inositol or d_6-MI) were purchased from C/D/N Isotopes.

Preparation of Proteins. Methods for overexpression and purification of the β_2 subunit of *Chlamydia trachomatis* (*Ct*) ribonucleotide reductase (RNR), *Da* Cld, *Escherichia coli* taurine:α-ketoglutarate (αKG) dioxygenase (TauD), *E. coli* (*Ec*) RNR-β_2, and *Mus musculus myo*-inositol oxygenase (MIOX) have been presented previously.[7,35,36,51,55] To prepare myoglobin (Mb) containing heme with natural abundance iron (^{56}Fe-Mb), 400 mg of lyophilized horse heart Mb (Sigma-Aldrich product no. M1882) was dissolved in 2 mL of 100 mM potassium phosphate buffer (pH 6.8). The protein was loaded onto a 50 mL anion exchange column (DE-52, Whatman) and eluted by gravity flow with the same buffer. Fractions with A_{409}/A_{280} ratios (R_z) of at least 5 were pooled and concentrated to a heme concentration of ∼10 mM. For ^{57}Fe-enriched heme (^{57}Fe-Mb), the synthesis of metalloporphyrin was adapted from that of Adler et al.[56] for ^{57}Fe heme enrichment. Apoprotein, generated using Teale's method,[57] was reconstituted at pH 7.[58] Excess heme was removed by anion exchange chromatography using Whatman DE-52 resin, as described above for ^{56}Fe-Mb. Fractions with R_z > 5 were pooled and concentrated to a heme concentration of ∼10 mM.

Stopped-Flow Absorption and Freeze-Quench EPR and Mössbauer Experiments. Procedures for the stopped-flow and freeze-quench experiments and the spectrometers for the stopped-flow, EPR, and Mössbauer measurements have been described previously.[7,34,36]

Analysis of the Stopped-Flow Absorption Kinetic Data. A_{390} versus time traces reflecting accumulation and decay of the Mn^{IV}/Fe^{IV} activation intermediate in *Ct*-RNR-β_2 were analyzed by nonlinear regression according to the equation

$$A_t = A_0 + \Delta A_1[1 - \exp(-k_1 t)] + \Delta A_2 [1 - \exp(-k_2 t)]$$

which gives absorbance as a function of time (A_t) for two irreversible first-order reactions in terms of the rate constants (k_1 and k_2), the amplitudes associated with each reaction (ΔA_1 and ΔA_2), and the initial absorbance (A_0) at time zero. The formation of the intermediate and its decay are sequential processes, but their well-resolved rate constants ($k_1[O_2] \gg k_2$) make the assumption of parallel reactions acceptable. Simulation of these traces was conducted using KinTek Explorer (KinTek Corp.). The kinetic mechanism for Cld and the K_D for the Cld·ClO_2^- Michaelis complex that were assumed in the simulations are given in Results. Kinetic constants for the formation and decay of the intermediate acquired from the regression fits in Figure 1B were assumed in the simulations. k_{cat} values of 30,000, 60,000, 120,000, and

200,000 s^{-1} (panels A–D of Figure S2 of the Supporting Information, respectively) were assumed for Cld.

Analysis of EPR and Mössbauer Spectra for Quantifying the Mn^{IV}/Fe^{IV} Intermediate in *Ct* RNR-β_2. Double integration of first-derivative EPR signals was conducted using the graphing and analysis program KaleidaGraph (Synergy Software). Comparison to the corresponding double integral for the spectrum of a $Cu^{II}(ClO_4)_2$ standard with correction for the different *g*-values[59] permitted calculation of absolute spin concentration. The spectral contribution of mononuclear Mn^{II} was subtracted out by using the spectrum of a sample of apo β_2 to which a known amount of Mn^{II} had been added. The contribution from the $Fe_2^{III/IV}$ complex (**X**) was quantified by individually integrating the six peaks of the sextet signal of the Mn^{IV}/Fe^{IV} intermediate. The double integrals of five of the peaks (all except for the fourth, with which the spectrum of **X** overlaps) are identical within error. The difference between the area of the fourth peak and the average area of the other five peaks represents the contribution of **X** to the experimental spectrum, which corresponds to 6% of the total spin. For samples prepared by the freeze-quench method, the absolute spin concentration in the reaction solution depends also on the "packing factor", which is the fraction of the packed material that consists of the actual solution (the fraction not contributed by the frozen cryosolvent). The spin concentration determined from comparison of the double integral of samples to that of the standard is divided by this packing factor to account for dilution of the frozen sample by the cryosolvent. In our extensive experience using isopentane as the cryosolvent, we have repeatedly measured packing factors of 0.52–0.60.[31,34] Table S1 of the Supporting Information provides concentrations of the paramagnetic species determined over a range of packing factors of 0.50–0.60. The narrower range of 0.54–0.56, which agrees with the mean packing factor of 0.55 that we have determined over many years, gives ranges of 1.24–1.16 and 0.13–0.11 mM for the concentrations of the Mn^{IV}/Fe^{IV} complex and **X**, respectively. These ranges are in good agreement with the values determined by analysis of the Mössbauer spectra.

The multiple Fe-containing species present in the freeze-quench samples all contribute to the experimental Mössbauer spectra, requiring that the spectra be "deconvoluted" into their components to extract the concentrations of species. However, the field orientation dependence of the predominant species, the Mn^{IV}/Fe^{IV} intermediate, provides an alternative means of accurate quantification. This analysis was conducted as previously described.[34] The slightly different spin Hamiltonian parameters used herein are provided in Table S2 of the Supporting Information and compared to the published values (given in parentheses[34]).

RESULTS

Activation of the β_2 Subunit of *Ct* RNR by Mixing Its Mn^{II}/Fe^{II} Complex with ClO_2^- in the Presence of Cld. We selected the activation reaction of the manganese- and iron-dependent class Ic *Ct* RNR as an ideal test case for the *in situ* generation of O_2 by the Cld/ClO_2^- system.[7,60,61] Previous studies showed that reaction of the Mn^{II}/Fe^{II} complex of the enzyme's β_2 subunit with O_2 results in formation of the catalytically functional Mn^{IV}/Fe^{III} cofactor[7,62,81] via a novel Mn^{IV}/Fe^{IV} activation intermediate.[34,63] The reaction is a kinetically well-behaved, two-step sequence, in which the first step, formation of the Mn^{IV}/Fe^{IV} intermediate, is cleanly first-order in O_2.[34] Both steps in the sequence are associated with absorbance changes, with the reactant complex being essentially transparent and the intermediate absorbing maximally at 390 nm with a molar absorptivity ($\varepsilon_{390} \sim 4500\ M^{-1}\ cm^{-1}$) approximately twice that of the Mn^{IV}/Fe^{III} product.[34] These characteristics permit convenient monitoring in stopped-flow absorption experiments.

Rapid mixing of a solution containing the *Ct* β_2 protein (200 μM dimer), Mn^{II} (3 equiv relative to β_2), Fe^{II} (1 equiv), and Cld (10 μM heme) with an equal volume of a 20 mM ClO_2^- solution (100 equiv relative to β_2; 2,000 equiv relative to Cld heme) results in a rapid increase in the absorbance at 390 nm (A_{390}) followed by its slower decay to approximately half of the maximal value (Figure 1A, black trace). The trace is qualitatively similar to that obtained by mixing the Mn^{II}/Fe^{II}–β_2 complex with O_2-saturated buffer (green trace). Analogous traces from control reactions from which either the Mn^{II}/Fe^{II}–β_2 reactant (blue trace), the ClO_2^- reactant (orange trace), or the Cld catalyst (red trace) was omitted do not show the characteristic behavior, suggesting that the transient behavior of the complete reaction reflects formation and decay of the Mn^{IV}/Fe^{IV} intermediate specifically as a result of the evolution of O_2 from ClO_2^- by Cld.

To verify that the complete reaction including the Mn^{II}/Fe^{II}–β_2 complex, Cld, and ClO_2^- produces the expected Mn^{IV}/Fe^{IV} activation intermediate, freeze-quench EPR and Mössbauer samples were prepared from a concentrated $Mn^{II}/^{57}Fe^{II}$–β_2 reactant solution (giving a final β_2 concentration of 1.88 mM with 1 equiv of $^{57}Fe^{II}$ and 2 equiv of Mn^{II}). The Mössbauer and X-band EPR spectra of identical samples that were allowed to react for 1 s (near the time of maximal A_{390} in the black trace in Figure 1A) before being freeze-quenched are shown in Figure 2, and quantitative analysis of these spectra is summarized in Tables S1 and S2 of the Supporting Information. The spectra are dominated by the features of the Mn^{IV}/Fe^{IV} intermediate,[34] confirming that it is formed in high yield [1.2 ± 0.3 mM by EPR and 1.2 ± 0.2 mM (63 ± 8% of total Fe) by Mössbauer]. A small fraction of the $Fe_2^{III/IV}$ intermediate, **X**, resulting from reaction of O_2 with $Fe_2^{II/II}$ centers formed in competition with the desired Mn^{II}/Fe^{II}–β_2 reactant complex, is also detected [0.2 ± 0.1 mM by EPR and 0.2 ± 0.1 mM (13 ± 5% of total Fe) by Mössbauer]. The spectroscopic results thus establish that the Cld/ClO_2^- system does indeed support formation of the expected intermediate.

The stopped-flow absorption kinetic traces of Figure 1A suggest that the Mn^{IV}/Fe^{IV} intermediate forms much faster in the Cld/ClO_2^- reaction than in the O_2-saturated buffer reaction (compare black and green traces), consistent with a greater O_2 concentration in the former case. To evaluate the effective O_2 concentration more quantitatively, experiments were conducted with varying ClO_2^- concentrations (Figure 1B). Effective first-order rate constants (k_{obs}) for intermediate formation extracted by regression analysis of the A_{390} kinetic traces are linearly dependent on ClO_2^- concentration at ≤4 mM ClO_2^- (Figure 1C and Figure S1 of the Supporting Information). The slope of the line, corresponding to the effective second-order rate constant, agrees precisely with that obtained by direct variation of O_2 concentration by mixing with O_2-containing buffer (gray diamonds in Figure 1C). This result indicates that, at ≤4 mM ClO_2^-, the Cld completely converts ClO_2^- to O_2 and Cl^- sufficiently rapidly that it does not impose a lag phase on Mn^{IV}/Fe^{IV} intermediate formation (which would tend to diminish the

dx.doi.org/10.1021/bi201906x | *Biochemistry* 2012, 51, 1607–1616

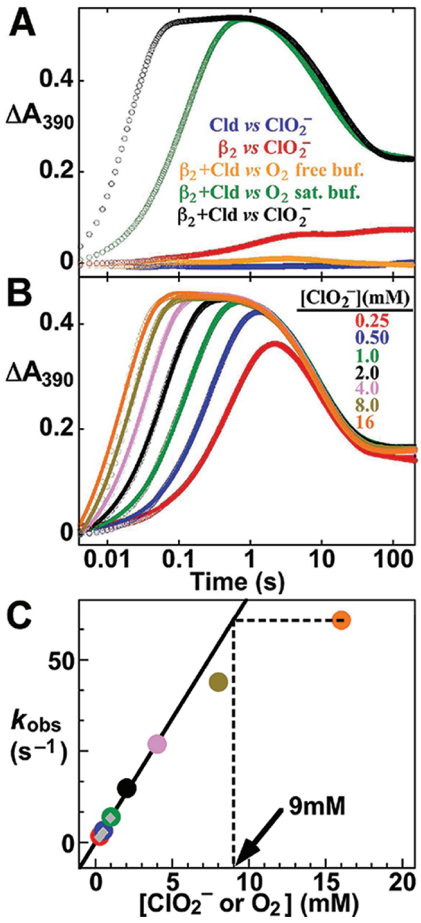

Figure 1. Activation of *Ct* β_2 using Cld and ClO_2^-. (A) The 390 nm absorbance vs time traces following rapid mixing at 5 °C of a solution containing 0.2 mM β_2, 0.6 mM Mn^{II}, 0.2 mM Fe^{II}, and 0.01 mM Cld with an equal volume of either 20 mM ClO_2^- (black trace), O_2-saturated 100 mM HEPES buffer (pH 7.6) (green trace), or O_2-free buffer (orange trace). Traces from control reactions, from which either Cld or β_2 was omitted, are colored red and blue, respectively. (B) Delineation of the O_2 concentration dependence of the *Ct* β_2 activation reaction by variation of ClO_2^- concentration. Reactions were conducted as described for the black trace in panel A, but with the concentration of the ClO_2^- reactant solution varied to give the final ClO_2^- concentrations noted in the figure. Traces were analyzed by nonlinear regression using the equation for two exponential phases [solid lines through data (see the Supporting Information for analysis)] to extract observed first-order rate constants for formation of the Mn^{IV}/Fe^{IV} intermediate (k_{obs}). (C) Plot of these observed first-order rate constants vs ClO_2^- or O_2 concentration. The points at ≤4 mM ClO_2^- were fit by the equation for a line (—). Extrapolation of the k_{obs} for the reaction with 16 mM ClO_2^- to the linear fit line (---) in this case gave an effective O_2 concentration of 9 mM (arrow). The gray diamond points are values of k_{obs} obtained after mixing with either O_2-saturated buffer (as in panel A, green trace) or buffer prepared by diluting O_2-saturated buffer 2- or 4-fold with O_2-free buffer, which has been done in the past to define the O_2 concentration dependence of the reaction.

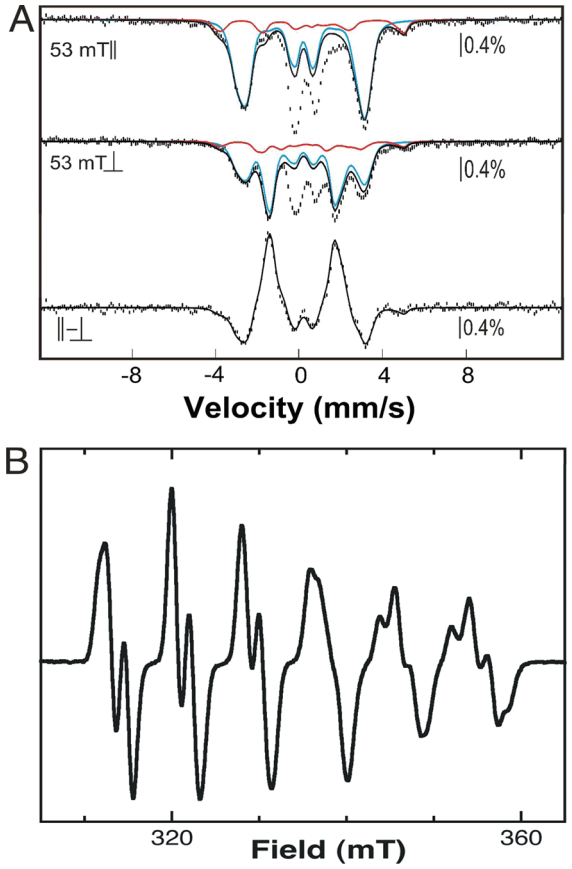

Figure 2. 4.2 K/53 mT Mössbauer and EPR spectra of *Ct* β_2 samples enriched in the Mn^{IV}/Fe^{IV} activation intermediate. The preparation of the samples is described in the text. (A) Experimental Mössbauer spectra were recorded with the magnetic field oriented parallel (top) or perpendicular (middle) to the γ beam, and the difference spectrum (bottom) was obtained mathematically. The solid blue and red lines are theoretical spectra of the Mn^{IV}/Fe^{IV} and $Fe_2^{III/IV}$ complexes, plotted at 63 and 13% of the total intensity, respectively. The theoretical spectrum of the $Fe_2^{III/IV}$ intermediate was generated with published parameters.[72] The parameters used to generate the theoretical spectrum of the Mn^{IV}/Fe^{IV} intermediate are slightly different from the previously published ones (see Table S2 of the Supporting Information). The spectrum shown matches the experimental difference spectrum more precisely than that generated with the published parameters and therefore permits more precise quantification. We attribute the need for these slight adjustments to the facts that the previously published parameters were obtained by "global" simulation of multiple spectra and the new spectra have a significantly better signal-to-noise ratio because they were collected on a more concentrated sample. (B) EPR spectrum showing that the predominant EPR-active species is the Mn^{IV}/Fe^{IV} intermediate. The spectrum of the contaminating $Fe_2^{III/IV}$ species (**X**) resulting from reaction of the $Fe_2^{II/II}$–β_2 complex with O_2 overlaps with the fourth line of the sextet and contributes 6% of the total spin (quantitative analysis of the spectrum is described in Experimental Procedures). Spectrometer conditions were as follows: 9.5 GHz microwave frequency, 20 μW microwave power, 14 ± 0.2 K temperature, 100 kHz modulation frequency, 10 G modulation amplitude, 167 s scan time, and 167 ms time constant.

extracted value of k_{obs}). At greater ClO_2^- concentrations, deviation from this strict first-order dependence is observed. Doubling the Cld concentration from 5 to 10 μM had no significant effect on the values of k_{obs} for ≤4 mM ClO_2^- but gave greater values (deviating less from the first-order dependence) at >4 mM ClO_2^- (Figure S1 of the Supporting Information). This observation suggests that the deviation is not intrinsic to the *Ct* β_2 reaction but rather reflects failure of the Cld reaction to rapidly reach completion at the higher ClO_2^- concentration. This conclusion is consistent with the chlorite-dependent destruction of the heme previously shown to limit turnover in the steady state.[53] Competition between

dx.doi.org/10.1021/bi201906x | *Biochemistry* 2012, 51, 1607–1616

Cld catalyst destruction and O_2 formation begins to manifest at 8 mM ClO_2^- [1,600 equiv of chlorite per Cld heme (Figure 1C)]. Extrapolation of the values of k_{obs} obtained at the highest ClO_2^- concentration tested (16 mM) to the fit line describing the first-order regime (dashed lines in Figure 1C and Figure S1 of the Supporting Information) indicates that effective O_2 concentrations of 7−11 mM were achieved in the stopped-flow experiments.

The kinetic traces of Figure 1B were simulated to assess limitations of the Cld/ClO_2^- system for *in situ* generation of O_2 and to extract an estimate of k_{cat} for Cld under these reaction conditions (Figure S2 of the Supporting Information). A simple rapid equilibrium binding kinetic model (Cld + ClO_2^- ⇆ Cld·ClO_2^- → Cl^- + O_2) with a value of K_D equal to the published value of K_M for ClO_2^- (215 μM) was assumed. The value of the rate constant for the single-step conversion of the bound substrate to free Cl^- and O_2 (equivalent to k_{cat} in this minimal kinetic scheme) was allowed to vary. k_{cat} values of ≤60,000 s^{-1} gave simulated traces with excessively pronounced lag phases and insufficiently rapid rises in A_{390} compared to the experimental traces (Figure S2 of the Supporting Information). k_{cat} values of ≥120,000 s^{-1} gave more acceptable agreement (Figure S2 of the Supporting Information) and are consistent with those measured in the steady state at pH ≤7. This extremely high turnover rate confirms that it should be possible to generate a >5 mM pulse of O_2 in <1 ms at the easily accessible Cld concentration of 50 μM.

Verification of a High Yield of O_2 from the ClO_2^-/Cld System by Monitoring Conversion of Fe^{II}-Myoglobin to Oxymyoglobin. To demonstrate the potential of using Cld to generate O_2 adducts at high concentrations, we selected myoglobin (Mb) as a very soluble and efficient O_2 receptor for which we could quantify the extent of reaction by Mössbauer spectroscopy.[64] Horse heart Mb was enriched to ~25% with ^{57}Fe. Fe^{II}-Mb was prepared by titration of the Fe^{III}-Mb with stoichiometric sodium dithionite. To preclude prior redox equilibration of the concentrated Fe^{II}-Mb reactant with the dilute oxidized (Fe^{III}) Cld catalyst (which could inactivate the Cld), the reaction was conducted via a sequential mixing protocol. The Fe^{II}-Mb and Cld solutions were mixed first. After being passed through a short connecting hose, this solution was mixed with the ClO_2^- solution, and then freeze-quenched after ~15 ms. Comparison of the Mössbauer spectra of the Fe^{II}-Mb reactant solution (Figure 3, top) and the freeze-quenched reaction sample (Figure 3, bottom) reveals essentially quantitative (>98%) conversion of the 6.7 mM Fe^{II}-Mb to the oxy form (the arrows indicate the small contribution from the remaining reactant). The spectrum of a control sample in which the Fe^{II}-Mb was mixed directly with the ClO_2^- solution (i.e., from which Cld was omitted) reflects conversion of only 7 ± 3% of the Fe^{II}-Mb to oxy-Mb (Figure S3 of the Supporting Information), establishing that the conversion observed in the complete reaction results from Cld-catalyzed evolution of O_2. This ~7% conversion in the control sample could reflect either contact with atmospheric O_2 during the mixing and freeze-quenching procedures or the accumulation of O_2 in the ClO_2^- reactant solution as a result of a slow spontaneous breakdown process.[65] Regardless, the spectrum of the complete reaction sample indicates that the 25 μM Cld catalyst produced a minimum of 6.5 mM O_2 in ~15 ms. Thus, the Cld/ClO_2^- system appears to be capable of effectively eliminating O_2 solubility as an obstacle for the preparation of O_2-dependent reactive intermediates at high concentrations and purities.

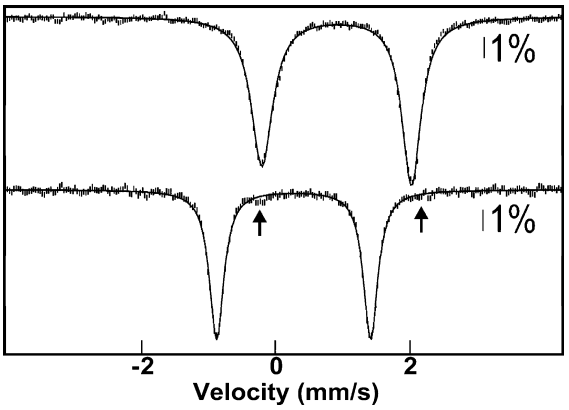

Figure 3. 4.2 K/53 mT (parallel field) Mössbauer spectra demonstrating conversion of ferrous Mb to oxy-Mb by the Cld/ClO_2^- system. A solution of 10 mM Mb (2.5 mM ^{57}Fe-Mb and 7.5 mM ^{56}Fe-Mb) was reduced with stoichiometric sodium dithionite (top spectrum). The Fe^{II}-Mb reactant was mixed with 0.25 equivalent volume of 0.125 mM Cld; this solution was mixed with 0.2 equivalent volumes of 100 mM ClO_2^-, and the complete reaction was freeze-quenched after 15 ms (bottom spectrum). The solid lines are quadrupole doublet simulations with parameters nearly identical to those previously published:[64] δ = 0.91 mm/s, and ΔE_Q = 2.23 mm/s (top); δ = 0.27 mm/s, and ΔE_Q = 2.29 mm/s (bottom).

Preparation of the Ferryl Intermediate, J, in *Ec* TauD at an Unprecedented Concentration. As an additional demonstration of the utility of the approach for preparing O_2-dependent reactive intermediates, we targeted the high-spin Fe^{IV}-oxo (ferryl) intermediate, **J**, which accumulates during O_2 activation by *Ec* TauD. **J** cleaves the C1−H bond of the substrate, taurine, with a rate constant of 13 s^{-1} at 5 °C and is stabilized significantly (k_{decay} = 0.35 s^{-1}) by inclusion of the deuterium-containing substrate, because of a large deuterium kinetic isotope effect.[33,66] Even with this increased half-life of ~2 s, the complex is still sufficiently short-lived that it must be prepared by rapid mixing methods. Thus, although **J** has been prepared at a high purity (~80%) and interrogated by several spectroscopic methods,[29,67,68] the maximal concentration of ~0.95 mM that has been obtained has precluded application of methods that require very high purity and concentration (e.g., NRVS). The ability to make more concentrated samples would make application of these methods feasible and afford the opportunity for further insight into the structure of **J**.

The Mössbauer spectrum of a sample prepared by mixing a solution containing the *Ec* TauD·Fe^{II}·αKG·d_4-taurine complex (6.0 mM TauD, 4.8 mM $^{57}Fe^{II}$, 10 mM αKG, and 10 mM d_4-taurine) with 0.25 equivalent volume of 120 μM Cld, mixing the resultant solution with 0.2 volume of a solution of 100 mM ClO_2^-, and then freeze-quenching the complete reaction after 0.03 s (Figure 4, vertical bars) is dominated by the sharp quadrupole doublet of **J** (blue line plotted above the data, accounting for 77% of the total absorption area of the experimental spectrum). The contribution of the spectrum of **J** corresponds to a concentration of 2.5 mM. Thus, the Cld/ClO_2^- system supports preparation of the intermediate at more than twice the maximal concentration achieved in previous studies and at a comparable purity.[29]

Preparation of the $Fe_2^{III/IV}$ Intermediate, X, of *Ec* RNR at an Unprecedented Concentration. As an additional demonstration of the utility of the approach for preparing O_2-dependent reactive intermediates, we targeted the $Fe_2^{III/IV}$

dx.doi.org/10.1021/bi201906x | *Biochemistry* 2012, 51, 1607−1616

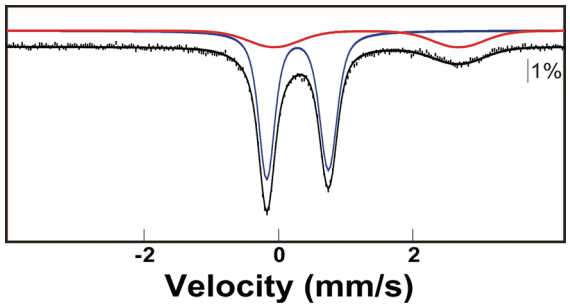

Figure 4. 4.2 K/53 mT (parallel field) Mössbauer spectrum of a freeze-quenched sample from the reaction of the TauD·Fe^{II}·αKG·d_4-taurine complex with the Cld/ClO_2^- system (see the text for details). The red line is a simulation of the spectrum of unreacted ferrous component (23%), the blue line is a simulation of the quadrupole doublet spectrum of **J** (δ = 0.29 mm/s, and $|\Delta E_Q|$ = 0.90 mm/s) accounting for 77% of the total intensity of the spectrum, and the solid black line is the summed contribution of both.

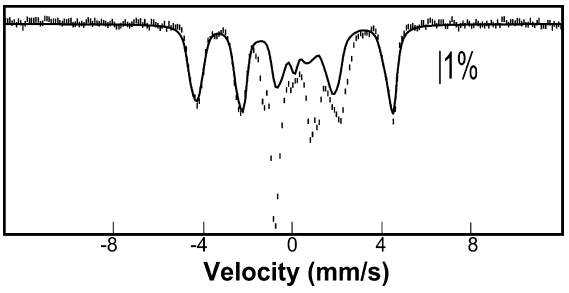

Figure 5. 4.2 K/53 mT (parallel field) Mössbauer spectrum showing accumulation of the $Fe_2^{III/IV}$ activation intermediate, **X**, in *Ec* RNR-β_2-Y122F mediated by the Cld/ClO_2^- system. A solution containing 2.6 mM *Ec* RNR-β_2-Y122F dimer, 7.41 mM $^{57}Fe^{II}$, 10 mM ascorbate, and 12.5 μM Cld was mixed with 0.25 equivalent volume of 50 mM ClO_2^-, and the reaction was freeze-quenched after 0.30 s. The solid line is the theoretical spectrum of **X** generated with published parameters[72] and plotted at 70% (2.0 mM) of the total absorption area of the experimental spectrum. The contributions from the $Fe_2^{II/II}$ and $Fe_2^{III/III}$ complexes represent 15% (each) of the total absorption area.

complex, **X**, that accumulates during activation of class Ia RNRs, including the most extensively studied ortholog from *Ec*.[27,28,35,45,69−72] **X** oxidizes a conserved tyrosine residue by one electron to a tyrosyl radical (which is essential for the activity of these RNRs[73]) as the diiron cluster is reduced to the μ-oxo-$Fe_2^{III/III}$ product.[5,35,71] Previous studies established that the complex has a half-life of ∼1 s at 5 °C and can be stabilized by ∼5-fold by substitution of the tyrosine that it oxidizes (Y122) with a redox inert phenylalanine.[35,71] Even with this increased lifetime in the Y122F variant, the complex is still sufficiently short-lived that it must be prepared by rapid mixing methods. As a result, the best samples yet reported have had a concentration of ≤0.77 mM at a purity of ≤68%.[45] Characterization of these optimized samples by EXAFS spectroscopy resulted in the report of an Fe−Fe distance of 2.5 Å,[45] much shorter than those reported in currently favored structural models.[27,28,69] The availability of more concentrated or purer (or both) samples would motivate re-examination of this crucial structural metric either to confirm it with renewed confidence or to revise it upward to a distance more compatible with structural models.[48,49]

The Mössbauer spectrum of a sample prepared by mixing a solution containing *Ec* RNR-β_2-Y122F (2.6 mM dimer), 7.41 mM $^{57}Fe^{II}$, 10 mM ascorbate, and 12.5 μM Cld with 0.25 equivalent volume of 80 mM ClO_2^- and freeze-quenching after 0.30 s (Figure 5, vertical bars) is dominated by the magnetic features of **X**. The solid line plotted over the data is the theoretical spectrum of **X** (generated with published parameters[72]) plotted at 70% of the total absorption area of the experimental spectrum. This contribution corresponds to a concentration of **X** of 2.0 mM. Thus, the Cld/ClO_2^- system supports preparation of the intermediate at more than twice the concentration achieved in previous studies and at a comparable purity.

Use of the Cld/ClO_2^- System To Drive the Reversible O_2 Addition Step Generating the Superoxo−$Fe_2^{III/III}$ Complex, G, in MIOX. A growing number of O_2-utilizing non-heme metalloenzymes are thought to employ midvalent metal−superoxo complexes, formed by the one-electron oxidative addition of O_2 to the reduced cofactors, to cleave C−H or C−C bonds (or both).[18,20,21,44,74−76] For only two such cases have the postulated superoxo complexes been directly detected.[43,77] For the unusual di-iron enzyme, *myo*-inositol (MI) oxygenase (MIOX),[55,75,77−79] it was shown that the reversible addition of O_2 to the $Fe_2^{II/III}$−MIOX·MI complex results in the formation of a putatively superoxo−$Fe_2^{III/III}$ complex, **G**, that cleaves the C1−H bond of MI to initiate its C−C bond-cleaving four-electron oxidation to D-glucuronate.[77] It was further shown that, even with the C−H bond cleavage step slowed by use of d_6-MI, the two pathways for decay of **G** (forward by C1−^{2}H bond cleavage at a rate of ∼48 s^{-1} and backward by reductive elimination of O_2 at a rate of ∼40 s^{-1}) conspire to make the net rate constant for its breakdown comparable to the effective first-order rate constant for its formation at the maximal accessible O_2 concentration of ∼1 mM (k ∼ 95 mM^{-1} s^{-1}, giving a k_{obs} of ∼95 s^{-1}), thereby limiting its maximal level of accumulation to ∼40% of the initial concentration of the reactant complex.[77] The inherent limitations on the concentration and purity of **G** imposed by the facile C−^{2}H bond cleavage and O_2 dissociation steps are largely responsible for the fact that its characterization has not progressed beyond the observation and analysis of its characteristic rhombic **g** = (2.06, 1.98, 1.92) EPR spectrum and ^{57}Fe nuclear hyperfine coupling thereupon. Moreover, it is likely that, for other enzyme reactions involving midvalent metal−superoxide complexes, high O_2 dissociation rates (perhaps in combination with efficient forward conversion steps) are responsible for having prevented the complexes from accumulating even to detectable levels.

To test whether the approach can be used to overcome a reversible O_2 addition step for the specific case of MIOX, thereby allowing greater accumulation of **G**, a solution containing the $Fe_2^{II/III}$−MIOX·MI complex was reacted with the Cld/ClO_2^- (20 μM/16 mM) system for the minimal accessible reaction time (transit time of 3 ms, total reaction time of ∼10 ms) before being freeze-quenched. Comparison of the EPR spectrum of this sample (Figure 6, red spectrum) to that of a control sample prepared by mixing the complex with 2 equivalent volumes of O_2-saturated buffer (giving an O_2 concentration of 1 mM) and freeze-quenching at the same reaction time (Figure 6, green spectrum) shows that the Cld/ClO_2^- system does permit **G** to accumulate to a greater extent: the resolved g = 2.06 and 1.92 features (green and black arrows) are ∼2-fold more intense in the spectrum of this sample than in that of the control. Moreover, the hallmark of

dx.doi.org/10.1021/bi201906x | *Biochemistry* 2012, 51, 1607−1616

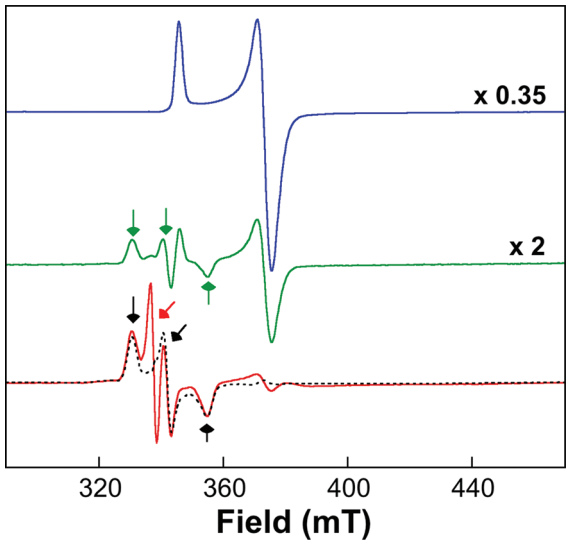

Figure 6. EPR spectra showing accumulation of the C1−H bond-cleaving superoxo−$Fe_2^{III/III}$ intermediate, **G**, in the MIOX reaction with d_6-MI initiated by the Cld/ClO_2^- system. A solution containing 1.13 mM $Fe_2^{II/III}$−MIOX (3 mM total MIOX protein), 60 mM d_6-MI (blue spectrum), and 30 μM Cld was mixed either with 2 equivalent volumes of O_2-saturated 50 mM Bis-Tris chloride (pH 6.0) buffer (green spectrum) or with 0.5 equivalent volume of a 48 mM ClO_2^- solution (red spectrum), and the reaction was freeze-quenched at a reaction time of ∼10 ms. The spectrometer conditions were as follows: 9.5 GHz microwave frequency, 100 kHz modulation frequency, 10 G modulation amplitude, 10 ± 0.2 K temperature, 100 μW power, 0.167 s time constant, and 10 scans per spectrum. The spectra were scaled as indicated to the right to account for dilution and packing factor (the fraction of the sample not contributed by the cryosolvent). The black, dashed line overlaid with the red spectrum is the published spectrum of **G**, acquired under similar spectrometer conditions. The green and black arrows indicate the g values of **G** (2.05, 1.98, and 1.91), whereas the red arrow indicates the organic radical signal present in the spectra of both reaction samples but featured more prominently in the Cld/ClO_2^- sample.

reversible and disfavored O_2 addition, a high level of the residual $Fe_2^{II/III}$−MIOX·MI complex (∼50% of the initial level) remaining after accumulation of **G** to its maximal extent, is quite evident in the spectrum of the control sample (g = 1.95 and 1.81 features; see the blue spectrum for their positions), but the magnitude of the associated signal is greatly diminished (by 15-fold) in the spectrum of the Cld/ClO_2^- sample. Both observations are consistent with the expected increase in O_2 concentration from ∼2.5 × K_D to ∼25 × K_D in **G** (K_D ∼0.4 mM) and the associated enhanced kinetic resolution of the formation and decay of the intermediate. Interestingly, a prominent g = 2.0 signal corresponding to ∼80 μM total spin is also observed in the spectrum of the Cld/ClO_2^- sample (red arrow). Although much less intense, this signal is, nevertheless, still evident in the spectra of the (−ClO_2^-/+O_2) control sample and an otherwise identical sample from which Cld was omitted. The g = 2.0 signal is thus associated with the MIOX reaction rather than the Cld/ClO_2^- reaction and could reflect accumulation of a substrate-based radical. Determining whether this previously undetected radical is an on-pathway intermediate that accumulates to a greater extent as a consequence of the greater accumulation of **G** or is an off-pathway species that forms in a side reaction that is favored by very high O_2 concentrations will require more extensive kinetic studies to correlate the changes observed by EPR with formation of MI-derived intermediates and products. Irrespective of the answer, the greater accumulation of **G** and diminution of residual $Fe_2^{II/III}$−MIOX·MI reactant should facilitate further characterization of **G**. More generally, the results illustrate the capacity of the Cld/ClO_2^- system to overcome the obstacle presented by an O_2 addition equilibrium that is unfavorable at the O_2 concentrations that can be accessed by conventional methods and equipment.

DISCUSSION

The Cld/ClO_2^- system can be used for rapid generation of concentrations of O_2 exceeding the normally achievable value of 2 mM to drive accumulation of metalloenzyme intermediates and surmount reversible and disfavored equilibria in the O_2 addition steps that initiate the reactions of some enzymes in this class. In addition to allowing for preparation of intermediate complexes that have already been identified, such as the Mn^{IV}/Fe^{IV} activation intermediate in *Ct* RNR and the H•-abstracting ferryl− and superoxo−$Fe_2^{III/III}$ complexes in TauD and MIOX, respectively, at concentrations and purities required for well-established and developing approaches to structural characterization (e.g., EXAFS and NRVS), this method could permit identification of previously undetected precursors to known complexes, thus further resolving the complex reaction pathways of these enzymes. For example, the reactions of the αKG-dependent oxygenases and the pterin-dependent aromatic amino acid hydroxylases are known to proceed through ferryl complexes that form rapidly without demonstrated accumulation of precursor complexes.[17] In the former enzymes, ferryl formation involves addition of O_2, cleavage of both the O−O bond of O_2 and the C1−C2 bond of αKG, and formation of a new C2−O bond in the succinate coproduct. Similarly, in the pterin-dependent enzymes, ferryl formation requires O_2 addition, O−O bond cleavage, and formation of a new C4a−O bond to the pterin. The kinetic masking of precursors leaves the pathways to ferryl formation experimentally unresolved. With O_2 concentrations greater by as much as 10-fold, addition of O_2 should occur 10 times more rapidly, perhaps permitting accumulation and identification of ferryl precursors. Alternatively, the failure of precursors to accumulate might reflect the reversible addition of O_2 to produce adducts with relatively high dissociation constants (≫1 mM). This situation is also likely in cases for which the initial adducts are proposed to effect difficult H• abstraction steps, as in MIOX. Here again, the ability to access ∼10 mM O_2 could permit this obstacle to be overcome. In many characterized reactions, including those of the αKG-dependent oxygenases, acceleration of the initial step would necessarily move the reaction times at which precursors accumulate to ≪10 ms, a regime that cannot be accessed by conventional cryosolvent-based freeze-quenching. In these cases, the recently developed "microsecond freeze-hyperquenching" technique[80] should permit the reactions to be terminated at these shorter times.

Two crucial requirements for the successful application of the system are the extraordinarily high efficiency of the Cld catalyst and the modest reactivities of target enzymes to ClO_2^-. These characteristics combine to ensure that the vastly predominant pathway is evolution of O_2 by the Cld catalyst and then reaction of O_2 with the target enzyme. The high efficiency of the Cld also requires that it not be strongly inhibited by components of the target enzyme reaction, such as by reduction or

dx.doi.org/10.1021/bi201906x | *Biochemistry* 2012, 51, 1607−1616

coordination to its Fe^{III}–heme cofactor.[53] The potential for this complication is minimized by a sequential mixing protocol, which ensures that the Cld catalyst is exposed to the components of the target enzyme reaction for only a few milliseconds before the Cld is exposed to its substrate. In cases for which the target enzyme is more reactive to ClO_2^- or components of the reaction inhibit Cld, it may be important to increase the Cld concentration to maintain the homogeneity of the reaction pathway. Additionally, the catalyst concentration must be elevated in the presence of a very high ClO_2^- concentration to keep the ClO_2^-:heme ratio less than ~1,500 to prevent deleterious competition between chlorite-mediated degradation of the Cld heme and generation of O_2. This is likely to be an issue primarily when delivery of exact quantities of O_2 is desirable (for example, in kinetic studies). The *Da* Cld used herein is soluble to concentrations of at least 500 μM, so even with use of high target enzyme:Cld volume ratios (e.g., 4:1 in the Mb experiment) to minimize dilution of the target enzyme, Cld concentrations of >100 μM are readily accessible. Given estimates of the k_{cat} of Cld (>100,000 s^{-1}) and the reasonably low K_M for ClO_2^- of 215 μM, this Cld concentration is theoretically capable of generating a 10 mM pulse of O_2 in 1 ms. With these impressive parameters, it seems likely that the system will be robust and widely applicable.

■ ASSOCIATED CONTENT

Supporting Information

Figure showing k_{obs} for formation of the *Ct* RNR-β_2–Mn^{IV}/Fe^{IV} intermediate as a function of ClO_2^- concentration in three different experiments at two different Cld concentrations, simulations of the stopped-flow kinetic traces reflecting formation and decay of the Mn^{IV}/Fe^{IV} intermediate, tables summarizing analysis of Mössbauer and EPR spectra for quantification of the Mn^{IV}/Fe^{IV} intermediate in freeze-quenched samples, and the Mössbauer spectrum of a control freeze-quenched sample prepared by mixing Fe^{II}-Mb with ClO_2^- in the absence of Cld. This material is available free of charge via the Internet at http://pubs.acs.org.

■ AUTHOR INFORMATION

Corresponding Author

*(J.M.B.) Department of Chemistry, 336 Chemistry Building, University Park, PA, 16802. Phone: 814-863-5707. Fax: 814-865-2927. E-mail: jmb21@psu.edu. (C.K.) Department of Chemistry, 332 Chemistry Building, University Park, PA, 16802. Phone 814-865-6089. Fax: 814-865-2927. E-mail: ckrebs@psu.edu. (J.L.D.) Department of Chemistry and Biochemistry, 251 Nieuwland Hall, Notre Dame, IN, 46556. Phone: 574-631-2696. E-mail: Jennifer.DuBois.3@nd.edu.

Funding

This work was supported by the National Institutes of Health (Grant GM-55365 to J.M.B., C.K., and M.T.G., Grants DK-74641 and GM-69657 to J.M.B. and C.K., and Grant GM-090260 to J.L.D.) and the Alfred P. Sloan Foundation Minority Ph.D. Scholarship Program (to L.M.K.D.).

Notes

The authors declare no competing financial interest. The pET41a-cld construct used in this study (protein accession/PDB ID code 3Q08) has been submitted to and can be obtained from the PSI Biology Materials Repository (http://psimr.asu.edu/index.html). This plasmid encodes a truncated form of the Cld from *Dechloromonas aromatica* (full protein sequence accession number YP_285781.1) with improved solubility and heme-incorporation. Please contact Dr. Catherine Cormier (Catherine.Cormier@asu.edu) for use of this plasmid for research purposes. Please address inquiries for the lyophilized protein to be used for research purposes to J. DuBois at jduboisnd@gmail.com. A patent for Cld-mediated dioxygen generation is pending.

■ ACKNOWLEDGMENTS

This paper is dedicated to our friend Vincent Huynh, with whom we have often agonized over the low solubility of O_2.

■ ABBREVIATIONS

RNR, ribonucleotide reductase; *Ct*, *Chlamydia trachomatis*; *Ec*, *Escherichia coli*; *Da*, *Dechloromonas aromatica*; TauD, taurine:α-ketoglutarate dioxygenase; αKG, α-ketoglutarate; MIOX, *myo*-inositol oxygenase; DFT, density functional theory; EXAFS, extended X-ray absorption fine structure; NRVS, nuclear resonance vibrational spectroscopy; Cld, chlorite dismutase; EPR, electron paramagnetic resonance; d_4-taurine, 1,1,2,2-[$^2H_4$]-2-aminoethane-1-sulfonic acid; MI, *myo*-inositol or cyclohexan-(1,2,3,5/4,6)-*hexa*-ol; d_6-MI, 1,2,3,4,5,6-[$^2H_6$]-cyclohexan-(1,2,3,5/4,6)-*hexa*-ol.

■ REFERENCES

(1) Ferguson Miller, S., and Babcock, G. T. (1996) Heme/copper terminal oxidases. *Chem. Rev. 96*, 2889–2907.

(2) Sono, M., Roach, M. P., Coulter, E. D., and Dawson, J. H. (1996) Heme-containing oxygenases. *Chem. Rev. 96*, 2841–2887.

(3) Solomon, E. I., Brunold, T. C., Davis, M. I., Kemsley, J. N., Lee, S.-K., Lehnert, N., Neese, F., Skulan, A. J., Yang, Y.-S., and Zhou, J. (2000) Geometric and electronic structure/function correlations in non-heme iron enzymes. *Chem. Rev. 100*, 235–349.

(4) Hausinger, R. P. (2004) Fe(II)/α-ketoglutarate-dependent hydroxylases and related enzymes. *Crit. Rev. Biochem. Mol. Biol. 39*, 21–68.

(5) Atkin, C. L., Thelander, L., Reichard, P., and Lang, G. (1973) Iron and free radical in ribonucleotide reductase. Exchange of iron and Mössbauer spectroscopy of the protein B2 subunit of the *Escherichia coli* enzyme. *J. Biol. Chem. 248*, 7464–7472.

(6) Klinman, J. P., and Mu, D. (1994) Quinoenzymes in biology. *Annu. Rev. Biochem. 63*, 299–344.

(7) Jiang, W., Yun, D., Saleh, L., Barr, E. W., Xing, G., Hoffart, L. M., Maslak, M.-A., Krebs, C., and Bollinger, J. M. Jr. (2007) A manganese(IV)/iron(III) cofactor in *Chlamydia trachomatis* ribonucleotide reductase. *Science 316*, 1188–1191.

(8) Fitzpatrick, P. F. (2003) Mechanism of aromatic amino acid hydroxylation. *Biochemistry 42*, 14083–14091.

(9) Kershaw, N. J., Caines, M. E. C., Sleeman, M. C., and Schofield, C. J. (2005) The enzymology of clavam and carbapenem biosynthesis. *Chem. Commun.*, 4251–4263.

(10) Ivan, M., Kondo, K., Yang, H., Kim, W., Valiando, J., Ohh, M., Salic, A., Asara, J. M., Lane, W. S., and Kaelin, W. G. Jr. (2001) HIFα targeted for VHL-mediated destruction by proline hydroxylation: Implications for O_2 sensing. *Science 292*, 464–468.

(11) Jaakkola, P., Mole, D. R., Tian, Y.-M., Wilson, M. I., Gielbert, J., Gaskell, S. J., von Kriegsheim, A., Hebestreit, H. F., Mukherji, M., Schofield, C. J., Maxwell, P. H., Pugh, C. W., and Ratcliffe, P. J. (2001) Targeting of HIFα to the von Hippel-Lindau ubiquitylation complex by O_2-regulated prolyl hydroxylation. *Science 292*, 468–472.

(12) Tsukada, Y.-i., Fang, J., Erdjument-Bromage, H., Warren, M. E., Borchers, C. H., Tempst, P., and Zhang, Y. (2006) Histone demethylation by a family of JmjC domain-containing proteins. *Nature 439*, 811–816.

(13) Cloos, P. A. C., Christensen, J., Agger, K., Maiolica, A., Rappsilber, J., Antal, T., Hansen, K. H., and Helin, K. (2006) The

putative oncogene GASC1 demethylates tri- and dimethylated lysine 9 on histone H3. *Nature 442*, 307−311.
(14) Liu, X. F., and Theil, E. C. (2005) Ferritins: Dynamic management of biological iron and oxygen chemistry. *Acc. Chem. Res. 38*, 167−175.
(15) Baik, M.-H., Martin, N., Friesner, R. A., and Lippard, S. J. (2003) Mechanistic studies on the hydroxylation of methane by methane monooxygenase. *Chem. Rev. 103*, 2385−2419.
(16) Costas, M., Mehn, M. P., Jensen, M. P., and Que, L. Jr. (2004) Dioxygen activation at mononuclear nonheme iron active sites: Enzymes, models, and intermediates. *Chem. Rev. 104*, 939−986.
(17) Krebs, C., Galonić Fujimori, D., Walsh, C. T., and Bollinger, J. M. Jr. (2007) Non-heme Fe(IV)-oxo intermediates. *Acc. Chem. Res. 40*, 484−492.
(18) Kovaleva, E. G., Neibergall, M. B., Chakrabarty, S., and Lipscomb, J. D. (2007) Finding intermediates in the O_2 activation pathways of non-heme iron oxygenases. *Acc. Chem. Res. 40*, 475−483.
(19) Solomon, E. I., Sundaram, U. M., and Machonkin, T. E. (1996) Multicopper oxidases and oxygenases. *Chem. Rev. 96*, 2563−2605.
(20) Chen, P., and Solomon, E. I. (2004) Oxygen activation by the noncoupled binuclear copper site in peptidylglycine α-hydroxylating monooxygenase. Reaction mechanism and role of the noncoupled nature of the active site. *J. Am. Chem. Soc. 126*, 4991−5000.
(21) Klinman, J. P. (2006) The copper-enzyme family of dopamine β-monooxygenase and peptidylglycine α-hydroxylating monooxygenase: Resolving the chemical pathway for substrate hydroxylation. *J. Biol. Chem. 281*, 3013−3016.
(22) Massey, V. (1994) Activation of molecular oxygen by flavins and flavoproteins. *J. Biol. Chem. 269*, 22459−22462.
(23) Kovaleva, E. G., and Lipscomb, J. D. (2007) Crystal structures of Fe^{2+} dioxygenase superoxo, alkylperoxo, and bound product intermediates. *Science 316*, 453−457.
(24) Kovaleva, E. G., and Lipscomb, J. D. (2008) Intermediate in the O-O bond cleavage reaction of an extradiol dioxygenase. *Biochemistry 47*, 11168−11170.
(25) Karlsson, A., Parales, J. V., Parales, R. E., Gibson, D. T., Eklund, H., and Ramaswamy, S. (2003) Crystal Structure of Naphthalene Dioxygenase: Side-on Binding of Dioxygen to Iron. *Science 299*, 1039−1042.
(26) Neese, F. (2006) A critical evaluation of DFT, including time-dependent DFT, applied to bioinorganic chemistry. *J. Biol. Inorg. Chem. 11*, 702−711.
(27) Han, W. G., Liu, T. Q., Lovell, T., and Noodleman, L. (2005) Active site structure of class I ribonucleotide reductase intermediate X: A density functional theory analysis of structure, energetics, and spectroscopy. *J. Am. Chem. Soc. 127*, 15778−15790.
(28) Mitić, N., Clay, M. D., Saleh, L., Bollinger, J. M. Jr., and Solomon, E. I. (2007) Spectroscopic and electronic structure studies of intermediate **X** in ribonucleotide reductase R2 and two variants: A description of the Fe^{IV}-oxo bond in the Fe^{III}-O-Fe^{IV} dimer. *J. Am. Chem. Soc. 129*, 9049−9065.
(29) Sinnecker, S., Svensen, N., Barr, E. W., Ye, S., Bollinger, J. M. Jr., Neese, F., and Krebs, C. (2007) Spectroscopic and computational evaluation of the structure of the high-spin Fe(IV)-oxo intermediates in taurine:α-ketoglutarate dioxygenase from *Escherichia coli* and its His99Ala ligand variant. *J. Am. Chem. Soc. 129*, 6168−6179.
(30) Hitchman, M. L. (1978) *Measurement of Dissolved Oxygen*, Vol. *49*, Wiley, New York.
(31) Baldwin, J., Krebs, C., Ley, B. A., Edmondson, D. E., Huynh, B. H., and Bollinger, J. M. Jr. (2000) Mechanism of rapid electron transfer during oxygen activation in the R2 subunit of *Escherichia coli* ribonucleotide reductase. 1. Evidence for a transient tryptophan radical. *J. Am. Chem. Soc. 122*, 12195−12206.
(32) Price, J. C., Barr, E. W., Hoffart, L. M., Krebs, C., and Bollinger, J. M. Jr. (2005) Kinetic dissection of the catalytic mechanism of taurine:α-ketoglutarate dioxygenase (TauD) from *Escherichia coli*. *Biochemistry 44*, 8138−8147.
(33) Bollinger, J. M. Jr., and Krebs, C. (2006) Stalking intermediates in oxygen activation by iron enzymes: Motivation and method. *J. Inorg. Biochem. 100*, 586−605.
(34) Jiang, W., Hoffart, L. M., Krebs, C., and Bollinger, J. M. Jr. (2007) A manganese(IV)/iron(IV) intermediate in assembly of the manganese(IV)/iron(III) cofactor of *Chlamydia trachomatis* ribonucleotide reductase. *Biochemistry 46*, 8709−8716.
(35) Bollinger, J. M. Jr., Edmondson, D. E., Huynh, B. H., Filley, J., Norton, J. R., and Stubbe, J. (1991) Mechanism of assembly of the tyrosyl radical-dinuclear iron cluster cofactor of ribonucleotide reductase. *Science 253*, 292−298.
(36) Price, J. C., Barr, E. W., Tirupati, B., Bollinger, J. M. Jr., and Krebs, C. (2003) The first direct characterization of a high-valent iron intermediate in the reaction of an α-ketoglutarate-dependent dioxygenase: A high-spin Fe(IV) complex in taurine/α-ketoglutarate dioxygenase (TauD) from *Escherichia coli*. *Biochemistry 42*, 7497−7508.
(37) Galonić, D. P., Barr, E. W., Walsh, C. T., Bollinger, J. M. Jr., and Krebs, C. (2007) Two interconverting Fe(IV) intermediates in aliphatic chlorination by the halogenase CytC3. *Nat. Chem. Biol. 3*, 113−116.
(38) Korboukh, V. K., Li, N., Barr, E. W., Bollinger, J. M. Jr., and Krebs, C. (2009) A long-lived, substrate-hydroxylating peroxodiiron-(III/III) intermediate in the amine oxygenase, AurF, from *Streptomyces thioluteus*. *J. Am. Chem. Soc. 131*, 13608−13609.
(39) Matthews, M. L., Krest, C. M., Barr, E. W., Vaillancourt, F. H., Walsh, C. T., Green, M. T., Krebs, C., and Bollinger, J. M. Jr. (2009) Substrate-triggered formation and remarkable stability of the C-H bond-cleaving chloroferryl intermediate in the aliphatic halogenase, SyrB2. *Biochemistry 48*, 4331−4343.
(40) Rittle, J., and Green, M. T. (2010) Cytochrome P450 compound I: Capture, characterization, and C-H bond activation kinetics. *Science 330*, 933−937.
(41) Bollinger, J. M. Jr., Krebs, C., Vicol, A., Chen, S., Ley, B. A., Edmondson, D. E., and Huynh, B. H. (1998) Engineering the diiron site of *Escherichia coli* ribonucleotide reductase protein R2 to accumulate an intermediate similar to $\mathbf{H}_{peroxo}$, the putative peroxodiiron(III) complex from the methane monooxygenase catalytic cycle. *J. Am. Chem. Soc. 120*, 1094−1095.
(42) Saleh, L., Krebs, C., Ley, B. A., Naik, S., Huynh, B. H., and Bollinger, J. M. Jr. (2004) Use of a chemical trigger for electron transfer to characterize a precursor to cluster **X** in assembly of the iron-radical cofactor of *Escherichia coli* ribonucleotide reductase. *Biochemistry 43*, 5953−5964.
(43) Mbughuni, M. M., Chakrabarti, M., Hayden, J. A., Bominaar, E. L., Hendrich, M. P., Münck, E., and Lipscomb, J. D. (2010) Trapping and spectroscopic characterization of an Fe(III)-superoxo intermediate from a nonheme mononuclear iron-containing enzyme. *Proc. Natl. Acad. Sci. U.S.A. 107*, 16788−16793.
(44) van der Donk, W. A., Krebs, C., and Bollinger, J. M. (2010) Substrate activation by iron superoxo intermediates. *Curr. Opin. Struct. Biol. 20*, 673−683.
(45) Riggs-Gelasco, P. J., Shu, L., Chen, S., Burdi, D., Huynh, B. H., Que, L. Jr., and Stubbe, J. (1998) EXAFS characterization of the intermediate **X** generated during the assembly of the *Escherichia coli* ribonucleotide reductase R2 diferric tyrosyl radical cofactor. *J. Am. Chem. Soc. 120*, 849−860.
(46) Shu, L., Nesheim, J. C., Kauffmann, K. E., Münck, E., Lipscomb, J. D., and Que, L. Jr. (1997) An $Fe_2^{IV}O_2$ diamond core structure for the key intermediate **Q** of methane monooxygenase. *Science 275*, 515−518.
(47) Gherman, B. F., Baik, M.-H., Lippard, S. J., and Friesner, R. A. (2004) Dioxygen activation in methane monooxygenase: A theoretical study. *J. Am. Chem. Soc. 126*, 2978−2990.
(48) Hsu, H. F., Dong, Y. H., Shu, L. J., Young, V. G., and Que, L. (1999) Crystal structure of a synthetic high-valent complex with an $Fe_2(\mu\text{-}O)_2$ diamond core. Implications for the core structures of methane monooxygenase intermediate **Q** and ribonucleotide reductase intermediate **X**. *J. Am. Chem. Soc. 121*, 5230−5237.

(49) Xue, G. Q., Wang, D., De Hont, R., Fiedler, A. T., Shan, X. P., Münck, E., and Que, L. (2007) A synthetic precedent for the $[Fe_2(IV)(\mu\text{-}O)_2]$ diamond core proposed for methane monooxygenase intermediate **Q**. *Proc. Natl. Acad. Sci. U.S.A. 104*, 20713−20718.
(50) Bell, C. B., Wong, S. D., Xiao, Y. M., Klinker, E. J., Tenderholt, A. L., Smith, M. C., Rohde, J. U., Que, L., Cramer, S. P., and Solomon, E. I. (2008) A combined NRVS and DFT study of Fe-IV═O model complexes: A diagnostic method for the elucidation of non-heme iron enzyme intermediates. *Angew. Chem., Int. Ed. 47*, 9071−9074.
(51) Streit, B. R., and DuBois, J. L. (2008) Chemical and steady-state kinetic analyses of a heterologously expressed heme dependent chlorite dismutase. *Biochemistry 47*, 5271−5280.
(52) Coates, J. D., and Achenbach, L. A. (2004) Microbial perchlorate reduction: Rocket-fuelled metabolism. *Nat. Rev. Microbiol. 2*, 569−580.
(53) Streit, B. R., Blanc, B., Lukat-Rodgers, G. S., Rodgers, K. R., and DuBois, J. L. (2010) How Active-Site Protonation State Influences the Reactivity and Ligation of the Heme in Chlorite Dismutase. *J. Am. Chem. Soc. 132*, 5711−5724.
(54) Goblirsch, B., Kurker, R. C., Streit, B. R., Wilmot, C. M., and DuBois, J. L. (2011) Chlorite Dismutases, DyPs, and EfeB: 3 Microbial Heme Enzyme Families Comprise the CDE Structural Superfamily. *J. Mol. Biol. 408*, 379−398.
(55) Xing, G., Barr, E. W., Diao, Y., Hoffart, L. M., Prabhu, K. S., Arner, R. J., Reddy, C. C., Krebs, C., and Bollinger, J. M. Jr. (2006) Oxygen activation by a mixed-valent, diiron(II/III) cluster in the glycol cleavage reaction catalyzed by *myo*-inositol oxygenase. *Biochemistry 45*, 5402−5412.
(56) Adler, A. D., Longo, F. R., Kampas, F., and Kim, J. (1970) On the preparation of metalloporphyrins. *J. Inorg. Nucl. Chem. 32*, 2443−2445.
(57) Teal, F. W. (1959) Cleavage of Haem-Protein Link by Acid Methylketone. *Biochim. Biophys. Acta 35*, 543.
(58) Wagner, G., Perez, M., Toscano, W. A., and Gunsalus, I. (1981) Apoprotein Formation and Heme Reconstitution of Cytochrome P450cam. *J. Biol. Chem. 256*, 6262−6265.
(59) Aasa, R., and Vänngård, T. (1975) EPR signal intensity and powder shapes: A reexamination. *J. Magn. Reson. 19*, 308−315.
(60) Jiang, W., Xie, J., Nørgaard, H., Bollinger, J. M. Jr., and Krebs, C. (2008) Rapid and quantitative activation of *Chlamydia trachomatis* ribonucleotide reductase by hydrogen peroxide. *Biochemistry 47*, 4477−4483.
(61) Bollinger, J. M. Jr., Jiang, W., Green, M. T., and Krebs, C. (2008) The manganese(IV)/iron(III) cofactor of *Chlamydia trachomatis* ribonucleotide reductase: Structure, assembly, radical initiation, and evolution. *Curr. Opin. Struct. Biol. 18*, 650−657.
(62) Jiang, W., Bollinger, J. M. Jr., and Krebs, C. (2007) The active form of *Chlamydia trachomatis* ribonucleotide reductase R2 protein contains a heterodinuclear Mn(IV)/Fe(III) cluster with $S = 1$ ground state. *J. Am. Chem. Soc. 129*, 7504−7505.
(63) Jiang, W., Saleh, L., Barr, E. W., Xie, J., Gardner, M. M., Krebs, C., and Bollinger, J. M. Jr. (2008) Branched activation- and catalysis-specific pathways for electron relay to the manganese/iron cofactor in ribonucleotide reductase from *Chlamydia trachomatis*. *Biochemistry 47*, 8477−8484.
(64) Debrunner, P. G. (1989) Mössbauer spectroscopy of iron porphyrins. *Phys. Bioinorg. Chem. Ser. 4*, 137−234.
(65) Greenwood, N. N., and Earnshaw, A. (1997) *Chemistry of the elements*, 2nd ed., Butterworth Heinemann, Oxford, U.K.
(66) Price, J. C., Barr, E. W., Glass, T. E., Krebs, C., and Bollinger, J. M. Jr. (2003) Evidence for hydrogen abstraction from C1 of taurine by the high-spin Fe(IV) intermediate detected during oxygen activation by taurine:α-ketoglutarate dioxygenase (TauD). *J. Am. Chem. Soc. 125*, 13008−13009.
(67) Proshlyakov, D. A., Henshaw, T. F., Monterosso, G. R., Ryle, M. J., and Hausinger, R. P. (2004) Direct detection of oxygen intermediates in the non-heme Fe enzyme taurine/α-ketoglutarate dioxygenase. *J. Am. Chem. Soc. 126*, 1022−1023.
(68) Riggs-Gelasco, P. J., Price, J. C., Guyer, R. B., Brehm, J. H., Barr, E. W., Bollinger, J. M. Jr., and Krebs, C. (2004) EXAFS spectroscopic evidence for an Fe═O unit in the Fe(IV) intermediate observed during oxygen activation by taurine:α-ketoglutarate dioxygenase. *J. Am. Chem. Soc. 126*, 8108−8109.
(69) Shanmugam, M., Doan, P. E., Lees, N. S., Stubbe, J., and Hoffman, B. M. (2009) Indentification of Protonated Oxygenic Ligands of Ribonucleotide Reductase Intermediate X. *J. Am. Chem. Soc. 131*, 3370−3376.
(70) Stubbe, J. (2003) Di-iron-tyrosyl radical ribonucleotide reductases. *Curr. Opin. Chem. Biol. 7*, 183−188.
(71) Ravi, N., Bollinger, J. M. Jr., Huynh, B. H., Edmondson, D. E., and Stubbe, J. (1994) Mechanism of assembly of the tyrosyl radical-diiron(III) cofactor of *E. coli* ribonucleotide reductase. 1. Mössbauer characterization of the diferric radical precursor. *J. Am. Chem. Soc. 116*, 8007−8014.
(72) Sturgeon, B. E., Burdi, D., Chen, S., Huynh, B. H., Edmondson, D. E., Stubbe, J., and Hoffman, B. M. (1996) Reconsideration of **X**, the diiron intermediate formed during cofactor assembly in *E. coli* ribonucleotide reductase. *J. Am. Chem. Soc. 118*, 7551−7557.
(73) Stubbe, J., Nocera, D. G., Yee, C. S., and Chang, M. C. Y. (2003) Radical initiation in the class I ribonucleotide reductase: Long-range proton-coupled electron transfer? *Chem. Rev. 103*, 2167−2202.
(74) Bollinger, J. M. Jr., and Krebs, C. (2007) Enzymatic C-H activation by metal-superoxo intermediates. *Curr. Opin. Chem. Biol. 11*, 151−158.
(75) Bollinger, J. M. Jr., Diao, Y., Matthews, M. L., Xing, G., and Krebs, C. (2009) *myo*-Inositol oxygenase: A radical new pathway for O_2 and C-H activation at a nonheme diiron cluster. *Dalton Trans. 6*, 905−914.
(76) Cicchillo, R. M., Zhang, H. J., Blodgett, J. A. V., Whitteck, J. T., Li, G. Y., Nair, S. K., van der Donk, W. A., and Metcalf, W. W. (2009) An unusual carbon-carbon bond cleavage reaction during phosphinothricin biosynthesis. *Nature 459*, 871−874.
(77) Xing, G., Diao, Y., Hoffart, L. M., Barr, E. W., Prabhu, K. S., Arner, R. J., Reddy, C. C., Krebs, C., and Bollinger, J. M. Jr. (2006) Evidence for C-H cleavage by an iron-superoxide complex in the glycol cleavage reaction catalyzed by *myo*-inositol oxygenase. *Proc. Natl. Acad. Sci. U.S.A. 103*, 6130−6135.
(78) Charalampous, F. C., and Lyras, C. (1957) Biochemical studies on inositol. IV. Conversion of inositol to glucuronic acid by rat kidney extracts. *J. Biol. Chem. 228*, 1−13.
(79) Xing, G., Hoffart, L. M., Diao, Y., Prabhu, K. S., Arner, R. J., Reddy, C. C., Krebs, C., and Bollinger, J. M. Jr. (2006) A coupled dinuclear iron cluster that is perturbed by substrate binding in *myo*-inositol oxygenase. *Biochemistry 45*, 5393−5401.
(80) Cherepanov, A. V., and de Vries, S. (2004) Microsecond freeze-hyperquenching: development of a new ultrafast micro-mixing and sampling technology and application to enzyme catalysis. *Biochim. Biophys. Acta 1656*, 1−31.
(81) Dassama, L. M. K., Boal, A. K., Krebs, C., Rosenzweig, A. C., and Bollinger, J. M. Jr. (2012) Evidence That the β Subunit of *Chlamydia trachomatis* Ribonucleotide Reductase Is Active with the Manganese Ion of Its Manganese(IV)/Iron(III) Cofactor in Site 1. *J. Am. Chem. Soc. 134*, 2520−2523.